Structural and Electrochemical Study of New $LiNi_{0.5}Ti_xMn_{1.5-x}O_4$ Spinel Oxides for 5-V Cathode Materials

R. Alcántara, M. Jaraba, P. Lavela, and J. L. Tirado*

Laboratorio de Química Inorgánica, Universidad de Córdoba, Edificio C3, planta 1, Campus de Rabanales, 14071 Córdoba, Spain

Ph. Biensan, A. de Guibert, C. Jordy, and J. P. Peres

SAFT Direction de La Recherche, 111 Boulevard Alfred Daney, 33074 Bordeaux, France

Received February 20, 2003. Revised Manuscript Received April 9, 2003

New $LiNi_{0.5}Ti_xMn_{1.5-x}O_4$ ($0.05 \leq x \leq 0.6$) spinel oxide materials have been obtained. The cubic unit cell parameter increases with the substitution of manganese by titanium in the octahedrally coordinated 16d sites, as evidenced by X-ray and neutron diffraction studies. For Ti-free $LiNi_{0.5}Mn_{1.5}O_4$ up to $x = 0.10$, a decrease in the line broadening of the X-ray diffraction profiles is observed. For $x > 0.1$, X-ray line broadening and a progressive loss of resolution in the FTIR spectral profiles are observed. The presence of small amounts of Ti ($x = 0.05$ and 0.1) yields a net improvement of the electrochemical performance, whereas a deterioration of the reversible capacity is observed for large Ti contents. The electrochemical oxidation mechanism involves the appearance of two or three cubic phases with different lattice parameters, as evidenced by ex situ XRD of electrodes prepared at different depths of the first charge.

Introduction

Spinel oxides with general formula $LiM_xMn_{2-x}O_4$ (M = Cr, Fe, Ni, Co, Cu, etc.) have recently been studied as 5-V cathode materials for advanced lithium-ion batteries.[1−6] These high-voltage electrodes could avoid the problems of lithium electroplating on graphite-based anodes by using negative electrodes working significantly above 0 V, while preserving the high power delivery of the lithium-ion cell.[7] The electrochemical processes of $LiM_xMn_{2-x}O_4$ might involve changes in the oxidation state of M, as well as of Mn. Thus, the Ni^{2+}/Ni^{4+} redox couple is the cause of the plateau at ca. 4.8 V in $LiNi_{0.5}Mn_{1.5}O_4$.[3,4,7,8]

The mechanism of the electrochemical reactions of $LiMn_2O_4$ in the 4-V region have been the subject of several studies. In 1996, Xia and Yoshio[9] proposed a one-phase model during lithium insertion and extraction. Later, Yang et al.[10] showed in situ synchrotron X-ray diffraction evidence for the occurrence of three different cubic phases and two regions of two-phase coexistence in the $0 < x < 1$ composition range. It was also shown that increasing the charge−discharge rate could result in apparent changes in the intermediate phases detected by diffraction procedures.[10] More recently, Xia et al.[11] demonstrated the role of oxygen deficiency in the detection of the two-phase regions. For $LiNi_{0.5}Mn_{1.5}O_4$, we have recently reported the changes in phase composition during cell charge and discharge.[12] The presence of two cubic spinel phases in the charge branches below a certain lithium content was indicative of the redistribution of lithium from a deeply deinserted solid.

The aim of this study was to obtain new $LiNi_{0.5}Ti_xMn_{1.5-x}O_4$ solid solution materials with the goal of improving electrode performance. A detailed comparison between titanium-containing and $LiNi_{0.5}Mn_{1.5}O_4$ spinel oxides was carried out by determining the structural and microstructural properties. The phase mechanism of electrochemical lithium extraction−insertion reactions about 5 V was studied by recording ex situ diffraction spectra of the electrodes, to gain for a better understanding of the parameters involved in the electrochemical behavior.

* To whom correspondence should be addressed. Tel: +34 957 218637. E-mail: iq1ticoj@uco.es.

(1) Kawai, H.; Nagata, M.; Tabuchi, M.; Tukamoto, H.;. West, A. R *Chem. Mater.* **1998**, *10*, 3266.
(2) Ein-Eli, Y.; Howard, W. F., Jr.; Lu, S. H.; Mukerjee, S.; McBeen, J.; Vaughey, J. T.;. Thackeray, M. M. *J. Electrochem. Soc.* **1998**, *145*, 1238.
(3) Kawai, H.; Nagata, M.; Tukamoto, H.; West, A. R. *J. Power Sources* **1999**, *81−82*, 67.
(4) Ohzuku, T.; Takeda, S.; Iwanaga, M. *J. Power Sources* **1999**, *81−82*, 90.
(5) Kawai, H.; Nagata, M.; Kageyama, H.; Tukamoto, H.; West, A. R. *Electrochim. Acta* **1999**, *45*, 315.
(6) Alcántara, R.; Jaraba, M.; Lavela, P.; Tirado, J. L. *Chem. Mater.* **2003**, *15*, 1210.
(7) Xia, Y.; Sakai, T.; Fujieda, T.; Wada, M.; Yoshinga, H. *Electrochem. Solid-State Lett.* **2001**, *4*, A9.
(8) Zhong, Q.; Bonakdarpour, A.; Zhang, M.; Gao, Y.; Dahn, J. R. *J. Electrochem. Soc.* **1997**, *144*, 205.
(9) Xia, Y.; Yoshio, M. *J. Electrochem. Soc.* **1996**, *143*, 825.
(10) Yang, X. Q.; Sun, X.; Lee, S. J.; McBreen, J.; Mukerjee, S.; Daroux, M. L.; Xing, X. K. *Electrochem. Solid-State Lett.* **1999**, *2*, 157.
(11) Xia, Y.; Sakai, T.; Fujieda, T.; Yasng, X. Q.; Sun, X.; Ma, Z. F.; McBreen, J.; Yoshio, M. *J. Electrochem. Soc.* **2001**, *148*, A723.
(12) Alcántara, R.; Jaraba, M.; Lavela, P.; Tirado, J. L. *Electrochim. Acta* **2002**, *47*, 1829.

10.1021/cm034080s CCC: $25.00
Published on Web 05/21/2003

Experimental Section

Solid precursors of the $LiNi_{0.5}Ti_xMn_{1.5-x}O_4$ ($x = 0$, 0.05, 0.1, 0.2, 0.3, 0.4, and 0.6) compounds were obtained by precipitation from a solution in a 3:1 water/ethanol mixture of $Ni(NO_3)_2 \cdot 6H_2O$, $TiCl_4$, and $Mn(NO_3)_2 \cdot 4H_2O$, by the addition of a $LiOH \cdot H_2O$ solution with a 10% Li excess.[13,14] The slurry was stirred and heated in air to dryness. The fine powdered solid was further annealed at 400 °C under an air atmosphere. The low-crystallinity product was ground in an agate mortar and reannealed at 700 °C for 3 or 5 days or at 800 °C for 1 or 5 days in an air atmosphere.

X-ray powder diffraction (XRD) patterns were step-scan recorded (0.04° 2θ steps of 6 s) on a Siemens D5000 instrument, using Cu Kα radiation and a graphite monochromator. The refinement of unit cell parameters was carried out by a least-squares method. The electrodes for ex situ XRD were always prepared inside a glovebox, by carefully opening the cells, placing the products on a glass sample holder, and finally covering them with a plastic film to avoid exposure to air. Neutron diffraction experiments were carried out on the high-resolution D1A diffractometer of the Institute Laue-Langevin (ILL, Grenoble, France) with a wavelength of 1.911 40 Å, a step of 0.050 (°, 2θ), and a data acquisition time of 4 h for each sample. The results were refined with the FULPROF[15] program. Rietveld refinements of neutron diffraction data were carried out for $LiNi_{0.5}Ti_xMn_{1.5-x}O_4$ samples using the $Fd\bar{3}m$ space group, by allowing Li in 8a sites and statistically distributed Ni, Ti, and Mn in 16d sites.

The electrochemical behavior was tested using two-electrode Swagelok cells of the type $Li|LiPF_6(EC:DEC)|LiNi_{0.5}Ti_xMn_{1.5-x}O_4$. The electrodes were prepared as 10-mm-diameter pellets by pressing a mixture of 86% active oxide, 6% PVDF binder, 4% graphite (Merck), and 4% carbon black 4N (Strem) to improve the mechanical and electronic conduction properties. Lithium electrodes consisted of a clean 10-mm-diameter lithium metal disk. The commercial electrolyte solution [Merck LP40, 1 M $LiPF_6$ in a 1:1 w/w mixture of ethylene carbonate (EC) and diethyl carbonate (DEC)] was supported by porous glass−paper disks (Whatman). The electrochemical experiments were carried out using a multichannel MacPile II system. Potentiostatic intermittent titration technique (PITT) cycling experiments were performed by allowing 0.1-h current relaxations after each 10-mV voltage step. Galvanostatic experiments were carried out at a *C*/20 rate, i.e., one Li extracted from $LiNi_{0.5}Ti_xMn_{1.5-x}O_4$ in 20 h.

Results and Discussion

The X-ray diffraction (XRD) patterns of all $LiNi_{0.5}Ti_xMn_{1.5-x}O_4$ samples with $x \leq 0.6$ obtained in this work could be ascribed to high-purity spinel products. Only traces of $Li_xNi_{1-x}O$ impurities could be observed by very weak intensity reflections at ca. 43.7 and 63.6° 2θ, particularly for samples prepared at 800 °C. Figure 1 shows the XRD patterns of a selected set of samples annealed at 700 °C for 3 days, in which the $Fd\bar{3}m$ space group reflections have been indexed. The negligible intensity of the (220) lines can be attributed to the absence of transition metal ions in tetrahedral coordination (8a sites). For Ti-doped $LiMn_2O_4$, Pistoia et al.[16] discussed the possible tetrahedral vs octahedral coordination of Ti^{4+} ions and found that the higher capacity of these materials as compared to other doping ions agrees well with Ti^{4+} substituting for Mn^{4+} in octahedral sites. The octahedral coordination of titanium was also reported for Ti-substituted $LiMn_2O_4$.[17] It should be noted that no reactions above 4.6 V were observed for lithium cells using $Li[Li_{0.04}Ti_{0.49}Mn_{1.47}]O_4$ electrodes,[17] irrespective of the presence of lithium in 16d sites.[18,19]

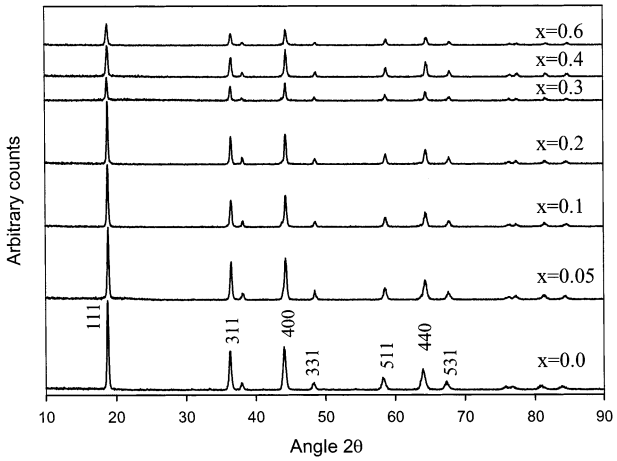

Figure 1. X-ray diffraction results for $LiNi_{0.5}Ti_xMn_{1.5-x}O_4$ samples for x equal to 0.0, 0.05, 0.1, 0.2, 0.3, 0.4, and 0.6.

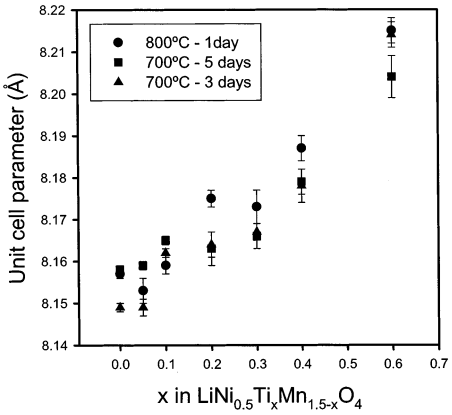

Figure 2. Changes in calculated cubic cell parameter with titanium content (x) for $LiNi_{0.5}Ti_xMn_{1.5-x}O_4$ samples obtained by heating at 700 °C for 3 or 5 days or at 800 °C for 1 day.

Indirect evidence for Ti/Mn substitution is obtained from the changes in unit cell parameter with composition. A continuous increase of the cubic cell parameter is observed in Figure 2, which can be interpreted in terms of the substitution of the smaller Mn^{4+} ions (67 pm) by Ti^{4+} (74.5 pm).[20] Better knowledge of the distribution of Ti atoms in the spinel sites was obtained from the results of Rietveld refinement of neutron diffraction patterns (Table 1). Slight deviations from the nominal stoichiometries were found, and the calculated amounts of titanium and nickel incorporated in the structure were slightly lower than the theoretical values. This is probably related to the presence of minor amounts of impurities. Moreover, the refined parameters clearly demonstrate that 8a site occupancy is always restricted to lithium ions. These results are in

(13) Arai, H.; Okada, S.; Ohtsuka, H.; Ichimura, M.; Yamaki, J. *Solid State Ionics* **1995**, *80*, 261.
(14) Alcántara, R.; Lavela, P.;. Tirado, J. L.; Stoyanova, R.; Kuzmanova, E.; Zhecheva, E. *Chem. Mater.* **1997**, *9*, 2145.
(15) Rodríguez-Carvajal, J. *Physica B* **1993**, *192*, 55.
(16) Pistoia, G.; Antonini, A.; Rosati, R.; Bellitto, C.; Ingo, G. M. *Chem. Mater.* **1997**, *9*, 1443.
(17) Shao-Horn, Y.;. Middaugh, R. L *Solid State Ionics* **2001**, *139*, 13.
(18) Tarascon, J. M.; McKinnon, W. R.; Coowar, F.; Bowmer, T. N.; Amatucci, G.; Guyomard, D. *J. Electrochem. Soc.* **1994**, *141*, 1421.
(19) Wang, X.; Iltchev, N.; Nakamura, H.; Noguchi, H.; Yoshio, M. *Electrochem. Solid-State Lett.* **2003**, *6*, A99.
(20) Shannon, R. D. *Acta Crystallogr.* **1976**, *A32*, 751.

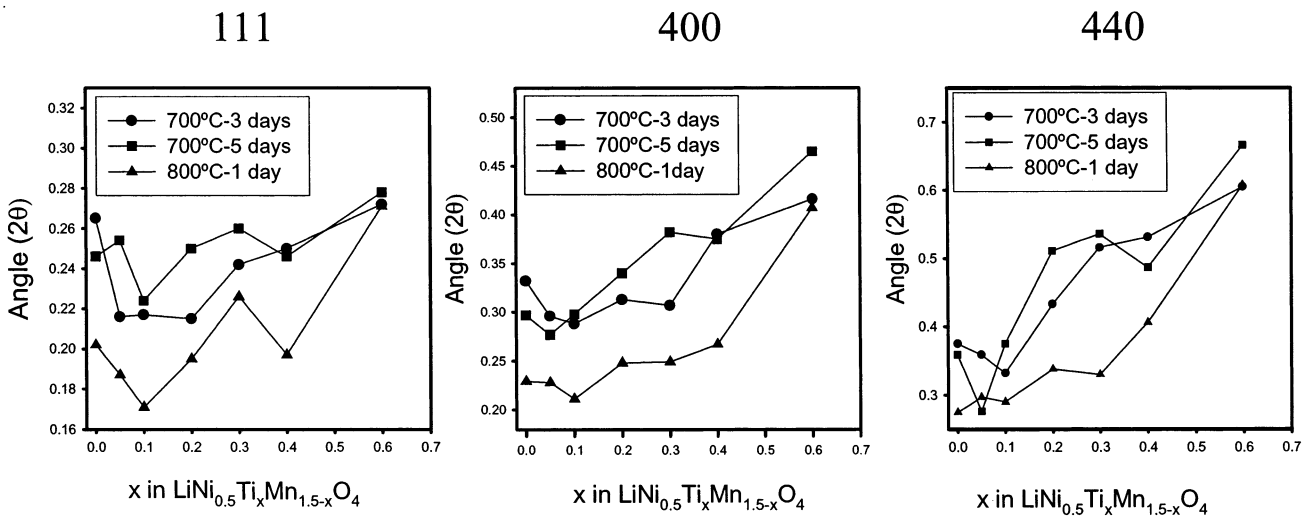

Figure 3. Plot of fwhm values of (111), (400), and (440) XRD reflections vs titanium content for $LiNi_{0.5}Ti_xMn_{1.5-x}O_4$ samples obtained at 700 and 800 °C.

Table 1. Results of Rietveld Refinements of Neutron Diffraction Data for $LiNi_{0.5}Ti_xMn_{1.5-x}O_4$ Samples Prepared at 800 °C for 5 Days[a]

cell parameter	atom	site	*x*	*y*	*z*	site occupancy	*B* iso
			$LiNi_{0.5}Mn_{1.5}O_4$				
8.153(1)	Li	8a	0.125	0.125	0.125	1.0	15.5
	Mn	16d	0.5	0.5	0.5	1.50	20.9
	Ni	16d	0.5	0.5	0.5	0.447	20.9
	O	32e	0.2626(3)	0.2626(3)	0.2626(3)	4.0	15.3
			$R_{Bragg} = 3.36$, $R_p/R_{exp} = 2.94$				
			$LiNi_{0.5}Ti_{0.1}Mn_{1.4}O_4$				
8.159(1)	Li	8a	0.125	0.125	0.125	1.0	15.9
	Mn	16d	0.5	0.5	0.5	1.430	35.8
	Ni	16d	0.5	0.5	0.5	0.458	35.8
	Ti	16d	0.5	0.5	0.5	0.082	35.8
	O	32e	0.2628(4)	0.2628(4)	0.2628(4)	4.0	15.2
			$R_{Bragg} = 3.42$, $R_p/R_{exp} = 2.57$				
			$LiNi_{0.5}Ti_{0.2}Mn_{1.3}O_4$				
8.185(1)	Li	8a	0.125	0.125	0.125	1.0	15.9
	Mn	16d	0.5	0.5	0.5	1.302	21.1
	Ni	16d	0.5	0.5	0.5	0.442	21.1
	Ti	16d	0.5	0.5	0.5	0.187	21.1
	O	32e	0.2627(3)	0.2627(3)	0.2627(3)	4.0	15.9
			$R_{Bragg} = 3.73$, $R_p/R_{exp} = 2.39$				
			$LiNi_{0.5}Ti_{0.4}Mn_{1.1}O_4$				
8.209(1)	Li	8a	0.125	0.125	0.125	1.0	15.0
	Mn	16d	0.5	0.5	0.5	1.108	30.4
	Ni	16d	0.5	0.5	0.5	0.484	30.4
	Ti	16d	0.5	0.5	0.5	0.390	30.4
	O	32e	0.2625(3)	0.2625(3)	0.2625(3)	4.0	14.4
			$R_{Bragg} = 4.19$, $R_p/R_{exp} = 2.94$				

[a] Space group is $Fd\bar{3}m$. $Z = 8$.

good agreement with a recent neutron diffraction study of mixed spinels.[21] The unit cell parameter obtained from neutron data agrees well with the X-ray results and evidence a Vegard's law tendency.

On the other hand, a comparison of the profiles of the different XRD diagrams in Figure 1, which were all obtained under the same scan conditions and for similar sample weights, reveals a general trend of decreasing intensity of the diffraction peaks and increasing line broadening when the titanium content exceeds $x = 0.10$. Both effects can be ascribed to a decrease in crystallinity and can be considered as resulting from the significant

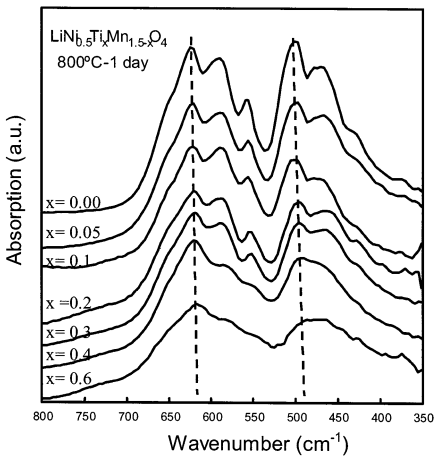

Figure 4. FTIR spectra of $LiNi_{0.5}Ti_xMn_{1.5-x}O_4$ samples for *x* equal to 0.0, 0.05, 0.1, 0.2, 0.3, 0.4, and 0.6.

lattice distortion induced by replacing smaller manganese atoms by larger titanium atoms. The line broadening effects were quantified by measuring the full width at half-maximum (fwhm) of the diffraction profiles. The fwhm values are plotted as a function of Ti content for three diffraction lines and different annealing temperatures in Figure 3. As the (111), (400), and (440) XRD reflections range from low to high scattering angles, these results might offer a clear picture of the crystallinity changes. The results in Figure 3 were very similar for the different crystallographic directions. However, the variation of the angle in fwhm as a function of *x* is smaller in the case of reflection (111), being less indicative when compared to the other two peaks. The initial decrease of the broadening up to $x = 0.1$ can be assigned to an increase in the size of the coherently diffracting domains, i.e., the presence of small amounts of Ti heteroatoms favors crystal growth, probably by releasing microstrains caused by lattice defects. Further Ti substitution leads to a progressive broadening and, hence, a decrease in the average domain size. The latter effect can be explained similarly by the above-mentioned difference between the Ti^{4+} and Mn^{4+} ionic radii.

FTIR spectroscopy was also used in the characterization of these samples. Figure 4 shows the spectra for

(21) Branford, W.; Green, M. A.; Neuman, D. A. *Chem. Mater.* **2002,** *14,* 1649.

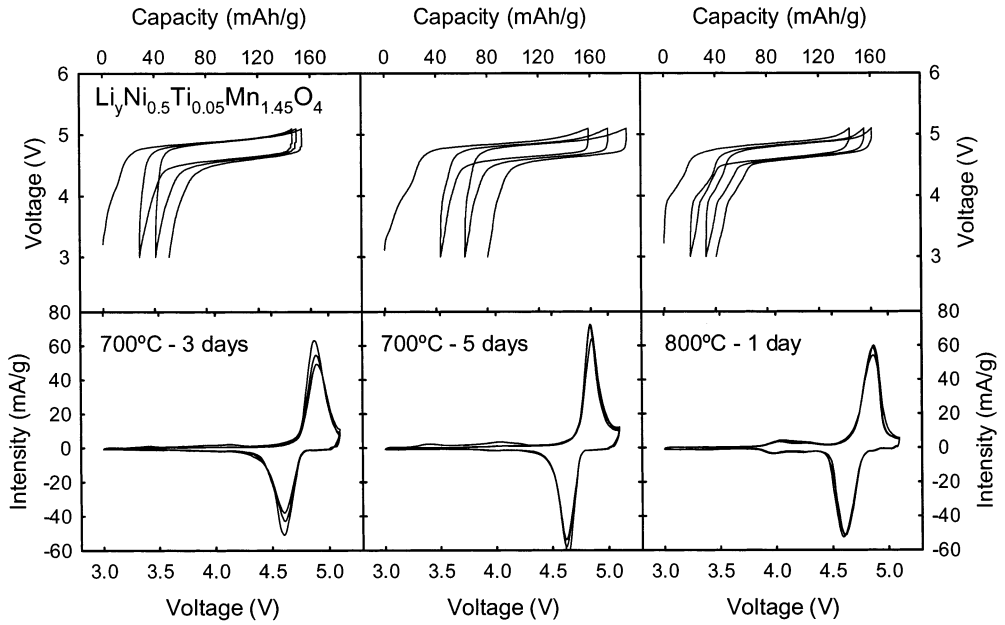

Figure 5. First three charge−discharge potentiostatic cycles of Li|$LiPF_6$(EC:DEC)| $LiNi_{0.5}Ti_{0.05}Mn_{1.45}O_4$ cells. Scan rate = 10 mV/0.1 h.

samples with up to 0.6 Ti per formula annealed at 800 °C for 1 day. The observed bands have been assigned according to the recent work of Ammundsen et al.[22] The two more intense bands can be attributed to two IR-active T_{1u} modes caused by metal−oxygen bond stretching. Moreover, several weak signals are detected. From the above-mentioned reference, these bands are theoretically inactive but are activated by the coupling of the vibrating atoms to the lattice. From Figure 4, the influence of Ti substitution on the FTIR spectra is revealed as a continuous smoothing of the profiles. This effect can be attributed to the above-mentioned loss of long-range ordering and the dispersion of the average metal−oxygen distances. The cation distribution is known to have a direct effect on the resolution of bands in IR spectra of spinel oxides. Preudhomnme[23] showed several examples in which the number of bands decreases with preparation temperature. The partial loss of long-range order discussed above and a random cation distribution could account for the loss of resolution in the spectra. A second effect that can be observed in these spectra is the shift of the band peaks on increasing Ti content. The observed decrease in wavenumber (see the lines used to guide the eye in Figure 4) with Ti content agrees well with the weakening of the bond strength, resulting from the increase in the average metal−oxygen distances caused by the presence of the larger Ti atoms in the lattice.

Figures 5 and 6 show the first three cycles obtained from PITT experiments on lithium cells using Ti-containing spinels as the active electrode material. The plots show the voltage vs capacity and weight-normalized intensity vs voltage curves for six selected samples: two compositions and three thermal treatments for each composition. Most of the cell capacity is exhibited in the 5-V region. It should be noted that, for $x = 0.05$ and 800 °C, Figure 5 shows a reversible cell capacity of 123 mA·h·g^{-1}, which is higher than that obtained for a $LiNi_{0.5}Mn_{1.5}O_4$ sample under the same experimental conditions (110 mA·h·g^{-1}), reported elsewhere.[12] Upon comparison of Figures 5 and 6, a pronounced change in curve shape is evident. Thus, a decrease in capacity, an increase in polarization, and steeper voltage/capacity curves are clearly detected for the sample with $x = 0.3$ and others with $x > 0.1$ (not shown). These effects can be explained by the microstructural properties discussed above. As the size of the crystalline domains is decreased, a larger surface reactivity with the electrolyte is expected that could deteriorate the values of the 5-V capacity and the electrochemical performance.

On the other hand, for $x = 0.05$ (Figure 5) and 0.10 (not shown), the PITT results show narrower oxidation and reduction peaks in comparison with those of $LiNi_{0.5}Mn_{1.5}O_4$ samples obtained under the same experimental conditions and reported elsewhere.[12] Similarly, the normalized intensity peak value is lower for the undoped material. However, a pronounced change in the curve shapes is evident from $x = 0.3$ (Figure 6). Thus, the decrease in capacity previously noted is accompanied by a decrease in maximum normalized intensity and an increase in broadening, and steeper voltage/capacity curves are clearly detected for these samples.

In addition, it should be noted the presence of a low-intensity 4-V reversible effect at 800 °C in Figures 5 and 6. This effect is associated with the higher unit cell parameter of samples prepared at 800 °C as compared with those prepared at 700 °C with $x > 0.1$ (Figure 2). This, in turn, is a consequence of the higher-temperature treatment, which induces significant oxygen loss.[8] Manganese reduction to Mn^{3+} is more prominent above $x = 0.1$, as is particularly clear from the larger unit cells of the samples prepared at 800 °C in Figure 2.

(22) Ammundsen, B.; Burns, G. R.; Islam, M. S.; Kanoh, H.; Rozière, J. *J. Phys. Chem. B* **1999**, *103*, 5175.
(23) Preudhomme, J. *Ann. Chim.* **1974**, *9*, 31.

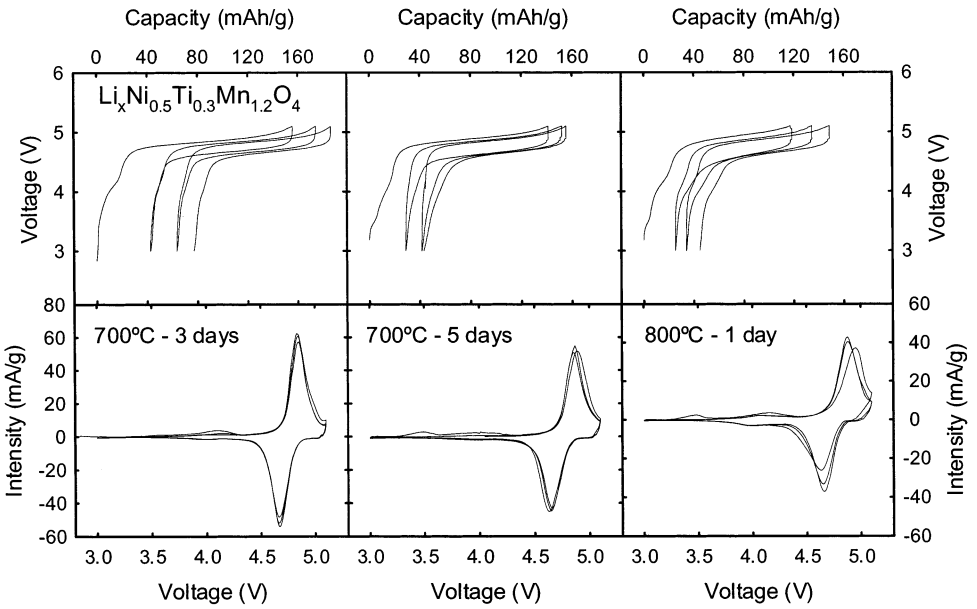

Figure 6. First three charge−discharge potentiostatic cycles of Li|$LiPF_6$(EC:DEC)| $LiNi_{0.5}Ti_{0.3}Mn_{1.2}O_4$ cells. Scan rate = 10 mV/0.1 h.

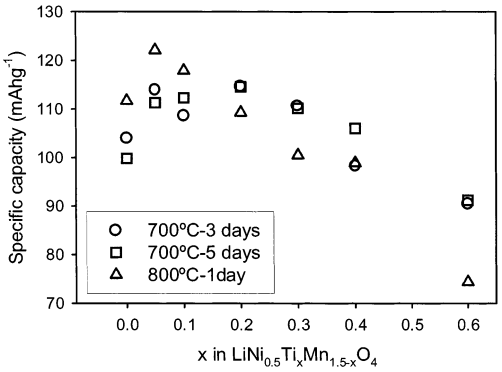

Figure 7. Total capacity of the second discharge as a function of titanium content.

A more extended view of the capacity as a function of Ti content, *x*, can be obtained from Figure 7. The total capacity values of the second discharge have a two-region dependence on the Ti content. Thus, an initial increase in cell capacity is observed upon addition of small amounts of titanium ($x = 0.05$ and 0.1). These results agree well with the above-discussed microstructural characterization and comments on Figure 5. In addition, Figure 7 shows that the highest capacity value in these series is obtained for 800 °C and $x = 0.05$.

Concerning capacity retention on successive cycles (Figure 8), it should be noted that, irrespective of the annealing temperature, all Ti-containing samples with $0 < x < 0.4$ showed a net improvement in capacity retention compared to the equivalent $LiNi_{0.5}Mn_{1.5}O_4$ sample. For samples annealed at 700 °C, the improvement in capacity retention is more marked for the $x = 0.2$ and 0.3 values. Again, the best results are obtained for a sample with $x = 0.05$ annealed at 800 °C, in which capacities higher than 120 $mA{\cdot}h{\cdot}g^{-1}$ are observed during nine cycles and close to this value after 20 cycles.

To gain deeper insight into the different electrochemical behavior of Ti-containing samples, additional information on the mechanism of the charge−discharge reaction of these materials was obtained. Galvanostatic recordings were interrupted at selected extensions of charge, and the electrode material was examined by ex situ X-ray diffraction recordings (Figures 9 and 10). The possible surface reactions between the electrodes charged to 5 V and the electrolyte were minimized by this procedure, as the cells were dismantled before the X-ray recordings. On the other hand, Yang et al.[10] recently discussed how high charge−discharge rates can result in multiphase regions being hidden. The galvanostatic experiments carried out in the present work prior to the ex situ XRD recordings used a sufficiently low rate (*C*/20) that allowed the observation of multiphase regions.

Figure 9 shows the changes with Ti content for the same extension of the cell charge process (nominally 0.1 Li per formula). These regions in the XRD pattern show splitted lines, which are clearly ascribable to multiphase products: three phases are clearly visible in Figure 9a and two in Figure 9b and c. This behavior partially agrees with that previously described for $Li_yNi_{0.5}Mn_{1.5}O_4$ prepared at 800 °C, in which a two-phase mechanism was reported.[12,24] The presence of three phases in Figure 9a suggests that the multiphase mechanism in this $Li_yNi_{0.5}Mn_{1.5}O_4$ spinel is affected by the annealing conditions used in the preparation of the material. These effects are also visible for Ti-containing samples (Figures 9−12). In contrast with Ni-containing solids, the partially oxidized $LiCo_xFe_yMn_{2-(x+y)}O_4$ electrodes recently studied showed single-phase products in the complete range of charge.[6]

For a particular Ti content, Figure 10 shows the complete XRD recordings of electrodes obtained at several charge−discharge depths. Again, the three phases involved in the charge process are clearly visible in a sample annealed at 700 °C. However, it is also clear that there are regions of lithium content in which only one or two phases are visible. In addition, Figure 10 shows that after a complete charge followed by a partial discharge to $y = 0.7$, a single-phase product is recovered,

(24) Myung, S. T.; Komaba, S.; Kumagai, N.; Yashiro, H.; Chung, H. T.; Cho, T. H. *Electrochim. Acta* **2002**, *47*, 2543

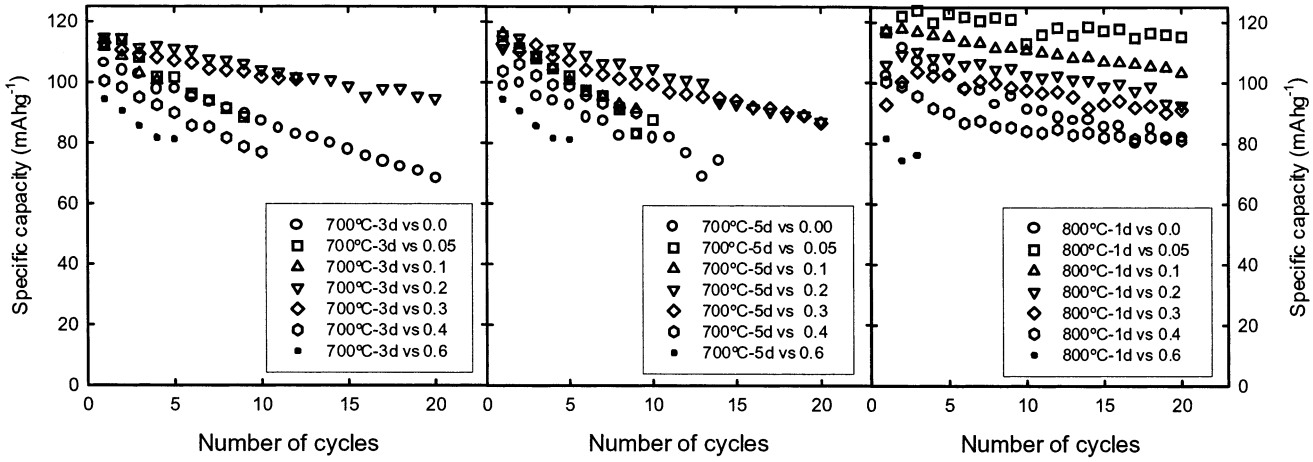

Figure 8. Capacity changes on PITT cycling between 3.1 and 5.1 V of Li|$LiPF_6$(EC:DEC)|$LiNi_{0.5}Ti_xMn_{1.5-x}O_4$ cells for cathodes obtained at (a) 700 °C, 3 days; (b) 700 °C, 5 days; and (c) 800 °C, 1 day.

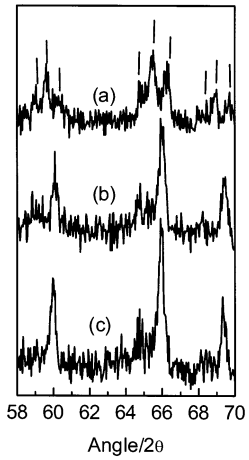

Figure 9. XRD of partially oxidized $Li_{0.1}Ni_{0.5}Ti_xMn_{1.5-x}O_4$ electrodes for (a) $x = 0.0$, 700 °C, 5 days; (b) $x = 0.05$, 800 °C, 1 day; and (c) $x = 0.1$, 800 °C, 5 days. Three phases are indicated with vertical lines in part a.

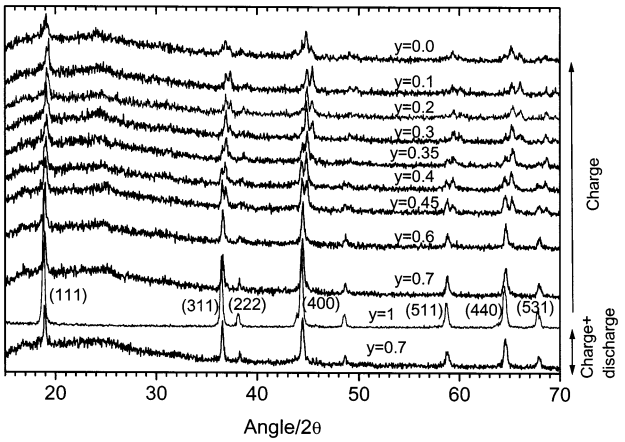

Figure 10. Ex situ XRD of electrodes containing $Li_yNi_{0.5}Ti_{0.1}Mn_{1.4}O_4$ prepared at 700 °C, 5 days, at different depths of the first charge and after a complete charge followed by a discharge to 4.0 V ($y = 0.7$).

thus indicating the very good reversibility of the structural changes taking place during the electrochemical process.

A complementary view of the multiphase process can be obtained by plotting the unit cell parameters of the different cubic spinel phases as a function of lithium

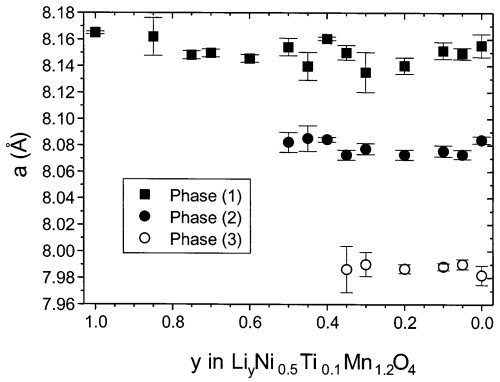

Figure 11. Calculated cell parameters of $Li_yNi_{0.5}Ti_{0.1}Mn_{1.4}O_4$ (700 °C, 5 days) electrodes at different depths of charge for electrodes.

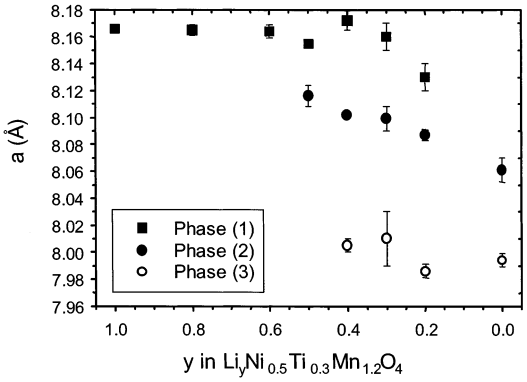

Figure 12. Calculated cell parameters of $Li_yNi_{0.5}Ti_{0.3}Mn_{1.2}O_4$ (700 °C, 5 days) electrodes at different depths of charge for electrodes.

content. Figures 11 and 12 show these results for samples with $x = 0.1$ and 0.3 after the lithium cell had been charged to different nominal y values in $Li_yNi_{0.5}Ti_xMn_{1.5-x}O_4$ assuming that no current was consumed in side reactions, e.g. electrolyte decomposition. From $y = 1$ to $y = 0.6$, Figures 11 and 12 show that the X-ray diffraction patterns can still be indexed in a single cubic phase. However, further lithium extraction caused the reflections to split, two cubic phases with different unit cell parameters can be detected from $y = 0.5$ to $y \approx 0.4$, and three phases to the complete extraction. The second phase shows a lower unit cell volume than the pristine

phase, similarly to that found in the deinserted phases emerging from $LiMn_2O_4$.[9−11] This can be explained by assuming that, from 1 to 0.6 lithium atoms per formula, the spinel structure can assimilate lithium extraction, whereas further extraction leads to the formation of separate domains, corresponding to each one of the two and finally three different ordered phases.

Conclusions

According to X-ray and neutron diffraction studies, titanium is incorporated into the $LiNi_{0.5}Ti_xMn_{1.5-x}O_4$ ($x \leq 0.6$) solid solutions, and the cubic unit cell parameter increases with the substitution of manganese by titanium in the octahedrally coordinated 16d sites.

The subsitution of small amounts of manganese by titanium in $LiNi_{0.5}Mn_{1.5}O_4$ leads to a net improvement of the reversible capacity and capacity retention in lithum cells. The changes in electrochemical performance were correlated with X-ray line broadening analysis, which reveals an increase of crystallinity with increasing cell capacity.

Ex situ XRD of partially oxidized electrodes provides evidence for a reversible multiphase mechanism. Two or three phases are visible with progressively lower lattice parameters.

Acknowledgment. The authors acknowledge financial support from the European Commission (Contract ENK6-CT2000-00082, Negelia) and CICYT (Contracts MAT2002-00434 and MAT2000-2721-CE). R.A. is indebted to MCYT (Programa Ramón y Cajal). Institute Laue-Langevin (ILL) of Grenoble is acknowledged for neutron diffraction facilities.

CM034080S